
RESEARCH ARTICLE

The Effect of Annealing Temperature on the Surface Roughness and Crystal Structure of ZnO Thin Films Prepared by Electron Beam Evaporation Method on Glass Substrate

Mohammad Arif Asim¹ ✉ and Bashir Ahmad Niazi²

^{1,2}Balkh University, Assistant Professor, Department of Physics, Faculty of Science, Balkh, Afghanistan

Corresponding Author: Mohammad Arif Asim, **E-mail:** arifasim1367@gmail.com

ABSTRACT

The investigation focused on studying the effect of annealing temperature on the surface morphology and crystalline structure of ZnO films. The Electron-beam evaporation method was used to prepare thin films of zinc oxide (ZnO) on glass substrates. The annealing process was conducted at temperatures of 200°C, 300°C, 400°C, and 500°C for the samples. The phase and crystal structure of the samples were determined using an X-ray diffraction (XRD) device. Additionally, the statistical parameters of surface roughness and morphological analysis of the layer's surface were calculated using an Atomic Force Microscope. The obtained results were analyzed using Gwyddion software and MATLAB coding. The x-ray diffraction analysis confirmed that the samples exhibit a similar pattern to the reference ZnO, and the crystallite size was found to be larger in the samples annealed at higher temperatures compared to those annealed at lower temperatures. The results obtained from both approaches were in excellent agreement, ensuring consistency in the characterization of surface roughness and indicating the presence of crystalline ZnO within the films. Moreover, higher annealing temperatures were observed to result in increased surface roughness, as confirmed by statistical methods and fractal analysis in the AFM analysis.

KEYWORDS

Surface roughness; Thin film; ZnO; Atomic force microscopy; crystallite, Annealing.

ARTICLE INFORMATION

ACCEPTED: 22 December 2023

PUBLISHED: 06 January 2024

DOI: 10.32996/ijbpcs.2024.6.1.1

1. Introduction

Nanostructured materials are characterized by having structural elements such as clusters, crystallites, or molecules with dimensions ranging from 1 to 100 nm (Xu et al., 2019). Recently, there has been a significant increase in the use of nanostructures and thin films in industry (Benelmekki & Erbe, 2019). This issue is caused by the diverse behavior of nanostructures compared to bulk materials. Meanwhile, oxide semiconductors have attracted the attention of researchers (Guermat et al., 2021 & Amakali et al., 2020). Zinc oxide (ZnO) is a nonorganic compound that takes the form of white powder and is insoluble in water (Chen et al., 2020 & Kayani et al., 2020). It is a semiconductor with a gap energy of 3.37eV, transparent in the visible wavelength range, and suitable for optoelectronic applications (Chen et al., 2020). ZnO is an extensively used functional material with a large exciton binding energy, excellent chemical and thermal stability, and optically visible transparency (Mehmood et al., 2021). The surface, the first boundary between matter and environment, plays a vital role in interacting matter and environment (Bukhari et al., 2019). Surface roughness greatly influences critical physical phenomena, such as mechanical contact (Hobson, 2019), sealing, adhesion, wave scattering, and friction (Xia et al., 2022). Layering another material on its surface can arbitrarily change some of the material's physical properties (Chen et al., 2020 & Ghule et al., 2006). Among the advantages of the coating method with electron beam evaporation is the possibility of adjusting the thickness of the coating, producing layers with uniform thickness and suitable hardness, and not harming the environment (Butt, 2020 & Borysiewicz, 2016). In this method, to reduce the collision between air molecules and sample atoms, it is necessary to use a vacuum environment to produce layers (Viswanathan et al, 2016). Most surfaces are rough, and the roughness of the interfaces can directly control many physical and chemical properties of the films

(Lee et al., 2003 & Henniges et al., 2013). This motivation can be studied as a random process. A surface for a particular application requires specified statistical properties. ZnO thin films have been prepared by many techniques, such as pulsed laser deposition (PLD), electron beam evaporation, magnetron sputtering, chemical vapor deposition (CVD), molecular beam epitaxy (MBE), and the sol-gel method (Abegunde et al., 2019). In another work, electron-beam physical vapor deposition (EBPVD) has produced thin zinc oxide films on a glass substrate. It employs atomic force microscopy (AFM) to investigate surface characterizations. Surface roughness, roughness exponents, and correlation length have been measured. ZnO thin film in different scales with glass substrate has been explicitly studied using fractal and multifractal formalism. Based on this, the surface growth and roughness of thin film are discussed.

2. Experimental details

The electron beam evaporation method is used for scattering layers with the dimensions of $1\mu\text{m}\times 1\mu\text{m}$ used in this research. All glass substrates were deposited under the same deposition conditions at room temperature. ZnO, with a purity of 99.99%, has been used as the target material (evaporation source). A quartz crystal controls the deposition rate to obtain layers with 150nm thickness at chamber vacuumed pressure of $3.5\cdot 10^{-5}$ mbar. To study the surface morphology and the effect of annealing temperature on grain size and roughness parameters, the layers were annealed at 200° C, 300° C, 400° C, and 500° C. The prepared samples, after annealing, were scanned with an atomic force microscope, and the obtained results were images with dimensions of $1\mu\text{m} \times 1\mu\text{m}$, which were analyzed with MATLAB software. The XRD method has investigated the samples' phase composition at an average temperature of $25^\circ < 2\theta < 80^\circ$ and $(2\theta/S) = 0.02$ step scanning.

3. Statistical analysis

This A rough surface can be described by its statistical properties through the $h(r)$ function [25]. This function can determine the deviation from a reference level at any point r . Therefore, $h(r)$ is the height of the points of the rough surface, and r is the position vector of the surface points; note that every point on the two-dimensional surface is determined by two spatial variables, x and y . The mean height of the character is a single-valued function of the position vector r . Surface roughness is a random parameter that describes the random field and is an n -dimensional probability density function of $p_n(h_1, h_2, \dots, h_n; r_1, r_2, \dots, r_n)$, where $r_1, r_2, r_3 \dots r_n$ is a set of different positions on the surface, and the $h_1, h_2, h_3 \dots h_n$ is the corresponding random variable (AverYanova et al., 2017).

The arithmetic mean height parameter is a global roughness parameter used to control the general quality of the surface.

$$R_a = \frac{1}{n} \sum_{i=1}^n |h_i| \quad (1)$$

RMS roughness shows the standard deviation of surface height distribution, which is more sensitive than the arithmetic mean of height.

$$R_q = \frac{1}{n} \sqrt{\sum_{i,j=1}^n (h_{(i,j)} - \langle h_{(i,j)} \rangle)^2} \quad (2)$$

The Skewness of a profile is the third central moment of the probability density distribution function of the profile domain. The Skewness of profiles with deep valleys is negative, and shapes with high peaks are favorable.

$$R_{sk} = \frac{1}{N \langle R_q \rangle^3} \sum_{i,j=1}^n (h_{(i,j)} - \langle h \rangle_N)^3 \quad (3)$$

The kurtosis parameter determines the degree of convergence of the curve peak of a statistical distribution concerning the normal distribution. If $R_{ku} < 3$, the distribution is Platycortic, and its peak is lower than the normal distribution; if it is greater than 3, the distribution is Liptocortic, and its height is higher than the normal distribution, and if it is equal to 3, the curve is called Mesocortic distribution, which shows the same as the normal distribution. Gives.

$$R_{ku} = \frac{1}{N \langle R_q \rangle^4} \sum_{i,j=1}^n (h_{(i,j)} - \langle h \rangle_N)^4 \quad (4)$$

The height-height correlation function can be expressed as:

$$H(md) = \frac{1}{N(N-m)} \sum_{j=1}^N \sum_{i=1}^N (h(i+m, j) - h(i, j))^2 \quad (5)$$

$$m = 0, 1, 2, \dots$$

For self-affine surfaces, the dynamic scaling hypothesis suggests that height-height correlation function $H(l)$ has the scaling form of:

$$H(l) = \begin{cases} (\rho l)^{2\alpha} & \text{for } l \ll l_0 \\ 2\omega^2 & \text{for } l \gg l_0 \end{cases} \quad (6)$$

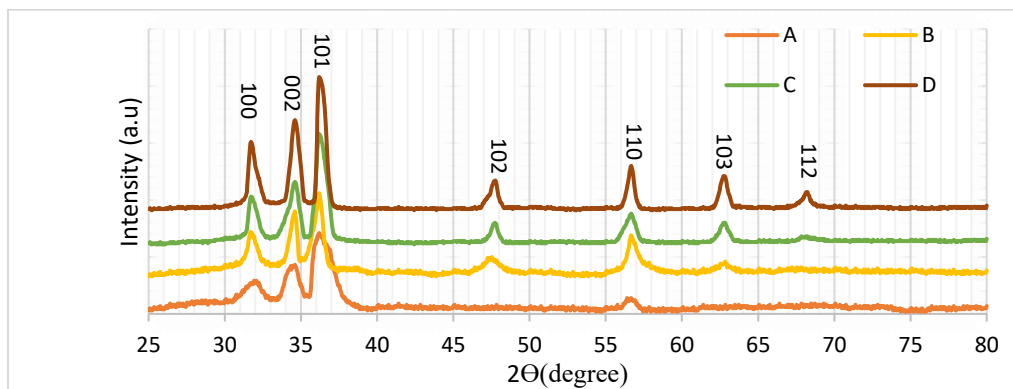
Where $\rho = \omega^{1/\alpha}/l_0$ is the local slope, α is the roughness exponent that describes how locally "wiggly" the sample surface is or to what degree the surface randomly fluctuates in a short range, and l_0 is the lateral correlation length, which is defined as the most considerable distance at which the height is still correlated. The roughness exponent, α , is directly related to the fractal dimension, Df , of the random surface by $Df = E + 1 - \alpha$, with $0 < \alpha < 1$, where $E + 1$ the size of the embedded space ($E = 1$ for profile; $E = 2$ for a plan).

The bearing area curve is a plot showing the distribution of contact pressure between two surfaces. It shows the percentage of the total contact area carrying a portion of the entire load (Salditt et al., 1995 & Manesh et al., 2010).

4. Results and Discussion

4.1 Structural properties of ZnO thin films

Figure 1 shows the XRD diffraction spectra of zinc oxide thin film samples annealed under different temperature conditions. The XRD outcome spectra show predominantly ZnO peaks, showing nature's Crystallinity, as shown in Figure 1. The ZnO nanostructures obtained are homogeneous and similar, which offer fine crystalline. Zinc oxide nanoparticles have been effectively synthesized in the Nano size scale.



All the samples have the highest peaks at an angle of approx 35°. Other graph peaks in other models are slightly different, especially in the fourth sample where the number of primes is more than others; it shows that the samples annealed at high temperature, the crystalline structure, and the Miller indices of the plates are easily accessible. These samples match well with standard card numbers 079-0207. The models have a hexagonal crystal structure in the $p63mc$ space group with group number 186; its unit cell parameters are listed in Table 1.

Table 1: The crystal lattice parameters of the samples obtained using XRD technique.

Crystal lattice parameters		Angles between sides	
a	$3.25 \pm 0.0054^\circ \text{ \AA}$	α	90°
b	$3.25 \pm 0.0054^\circ \text{ \AA}$	β	90°
c	$5.20 \pm 0.0054^\circ \text{ \AA}$	γ	120°

The preferred growth direction of the sample layers is plane (101). The differences seen in the values and FWHM of the samples with reference ZnO are caused by the stresses applied to the lattice and inherent crystal defects. The size of the crystals, depending on the dominant orientation, was calculated using Scherer's relation (Equation 7).

$$D = \frac{0.9\lambda}{\beta \cdot \cos\theta} \quad (7)$$

The size of the crystallites of the samples was calculated using the values of the diffraction angle 2θ , corresponding to the highest peaks (101), and the full width at half maximum related to the maximum intensity, which was established in the Scherer relationship, and are listed in Table 2. The results show that the crystallites' size increased with the annealing temperature of the samples.

Table 2 X-ray diffraction results and crystal size calculations in the samples obtained using Scherer's equation.

Simple	Highest peak	2θ	FWHM	Crystallite size [nm]
A	101	36.47	1.43	5.9
B	101	36.18	0.73	11.4
C	101	36.90	0.4329	15.6
D	101	34.21	1.2939	20.3

4.2 Atomic Force Microscopy Results

Typ Figure 2 (A-D) shows the three-dimensional Atomic Force Microscope images of the surface of ZnO thin films annealed at temperatures of 200°C, 300°C, 400°C and 500°C, respectively.

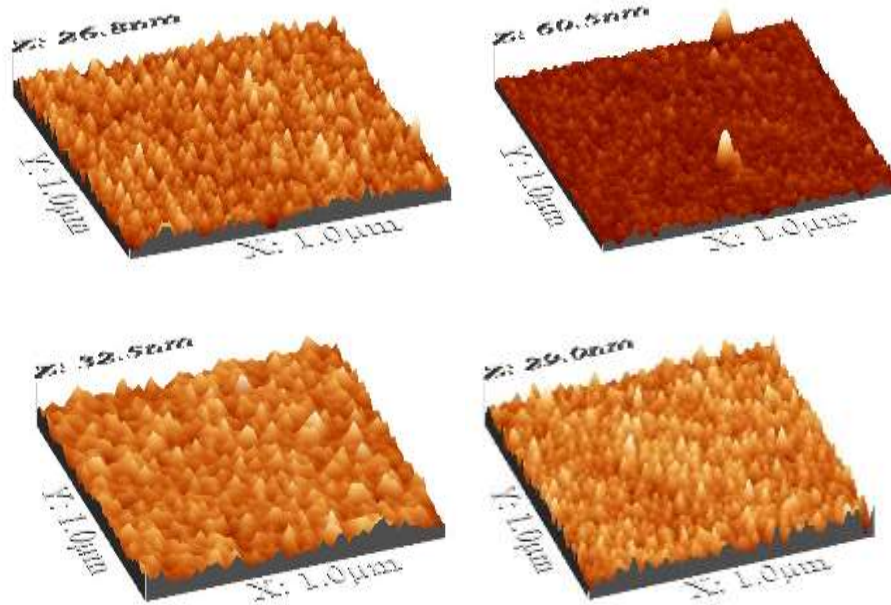


Figure 2 3D images of ZnO thin film surfaces taken by atomic force microscopy

According to Figure 2, the size of the surface of all samples is $1\mu\text{m} \times 1\mu\text{m}$, and the maximum height of the surface is 60.5, 28.8, 29.0 and 32.5 nm, respectively. The grain size of the surface annealed at higher temperatures appears coarser than samples that annealed at lower temperatures. The roughness of the samples was analyzed using an Atomic Force Microscope and MATLAB software (Figure 3), and the results are listed in Table 3. Histograms of height distributions, which are approximately Gaussian distributions, along with their normal distributions, are plotted in Fig. 3 (A-D).

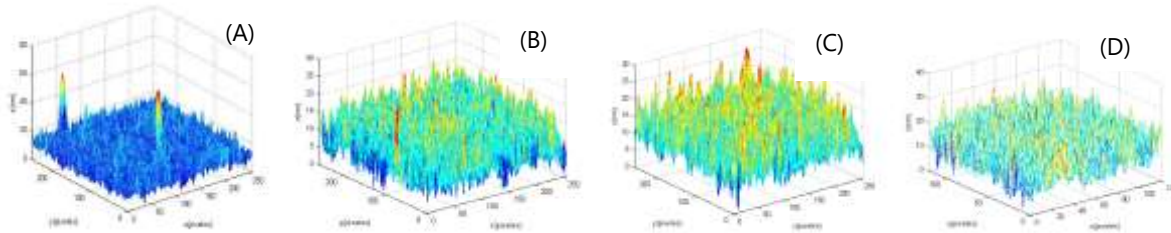


Figure 3 (A-D) Images of ZnO thin layers obtained with MATLAB software.

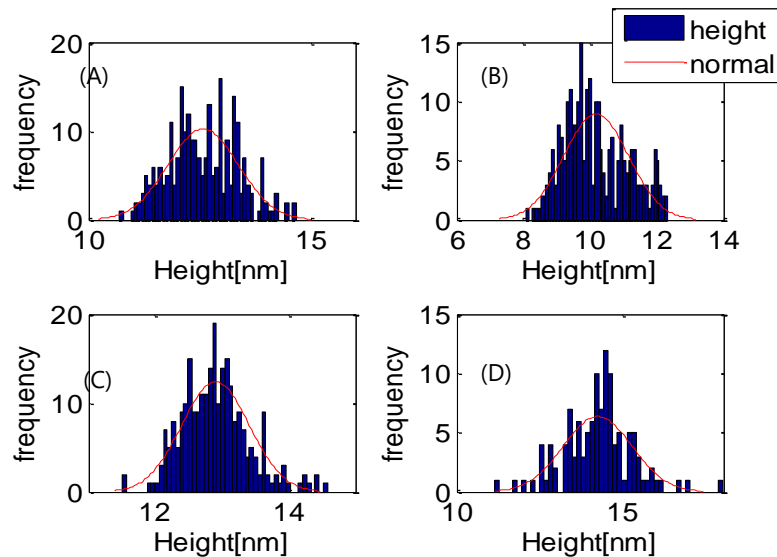


Figure 4 Histogram of the height distribution of the samples and the normal curve of each of them.

In Figures 4 (B) and 4 (C), a part of the distribution is placed to the left of the standard distribution curve, indicating negative skewness; that is, most sample materials are above the average level line. In Fig. 4 (D), a small part of the distribution is placed to the right of the standard distribution curve, which indicates positive skewness; that is, the majority of the sample materials are below the average level line, and in Fig. 4 (A), the sample distribution is almost consistent with the Gaussian (normal) distribution, that is, the distribution of particles is practically uniform.

Table 3: The results of the statistical parameters of the surface of the ZnO thin layer obtained by atomic force microscopy, which R_a shows the arithmetic mean of height, R_q RMS roughness, R_{sk} skewness and R_{ku} kurtosis.

Sample	R_{ku}	R_{sk}	R_q	R_a
A	3.2949	2.2513	3.9358	12.5756
B	3.1757	0.4230	3.2349	10.1805
C	3.1497	0.3515	3.4724	12.9024
D	3.1074	0.2960	4.0822	14.2280

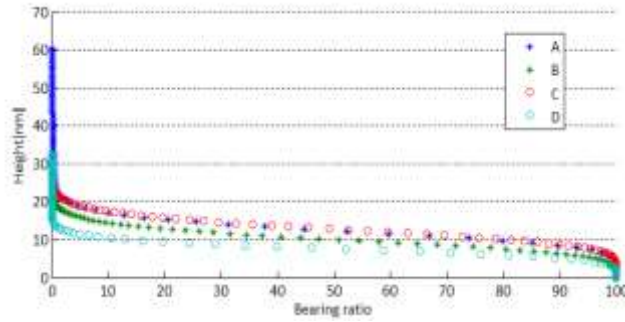


Figure 4 The tolerance bearing curve for sample surfaces

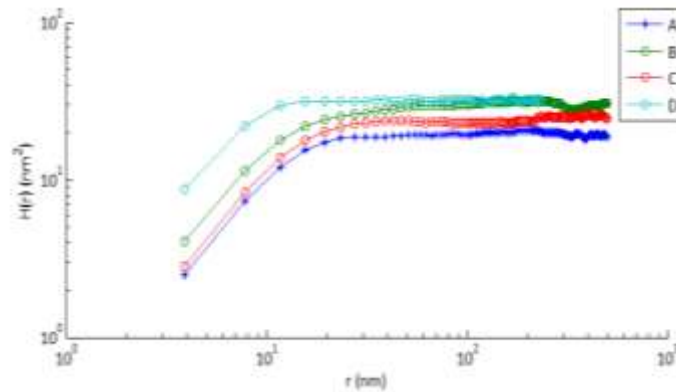


Figure 5 shows the height-height correlation function for all four samples.

As can be seen in the table, the samples annealed at higher temperatures have higher RMS roughness, and their skewness and kurtosis parameters are lower. It can be seen in Figure 4 that the particle distribution on the sample surfaces during the coating process is almost uniform, and about 80% of the data are located on the surface (mean line). Approximately 10% of the data are above the mean line, and another 10% are below the mean line, which has resulted in the creation of surface roughness.

The height-height correlation function graphs for the sample surfaces are shown in Figure 5. By fixing the charts and obtaining the intersection point between the smooth part of the curve and the inclined part of the graphs, the morphology of the surfaces is obtained according to equation (6). The results obtained for the RMS roughness parameter in Table 4-7, which were obtained using the statistical definition of this parameter, are consistent with the results presented in Table 4-8, which were obtained using fractal analysis of the surface of thin films. There is a minimal difference between them, which can be ignored.

Table 4 RMS roughness and fractal parameters of ZnO thin films

Samples	Annealing temperature	α	$R_q [nm]$	D_f
A	200°C	0.566	3.879	2.434
B	300°C	0.185	3.129	2.185
C	400°C	0.743	3.495	2.257
D	500°C	0.935	3.998	2.066

4.3 Surface profile roughness parameters

The surface of the mentioned samples with 11 dimensions scanned with an atomic force microscope was analyzed using Gwyddion software. The numerical results with the obtained images are included in this section. As shown in Figure 6, a slight bump can be seen on the surface of the layer, which may have been formed during the coating process or when scanning the surface due to its lack of cleanliness. The vertical profile of the layer is between 0.6 and 0.8 micrometers. A relatively high peak can be seen, which can affect the numerical results of the roughness parameters of the profile. The statistical parameters of the vertical profile

compared to the horizontal profile in the fourth sample also have higher values, and the reason for this depends on the selection of the shape's position on the layer level. With changes in the part of the profile, its statistical parameters also change.

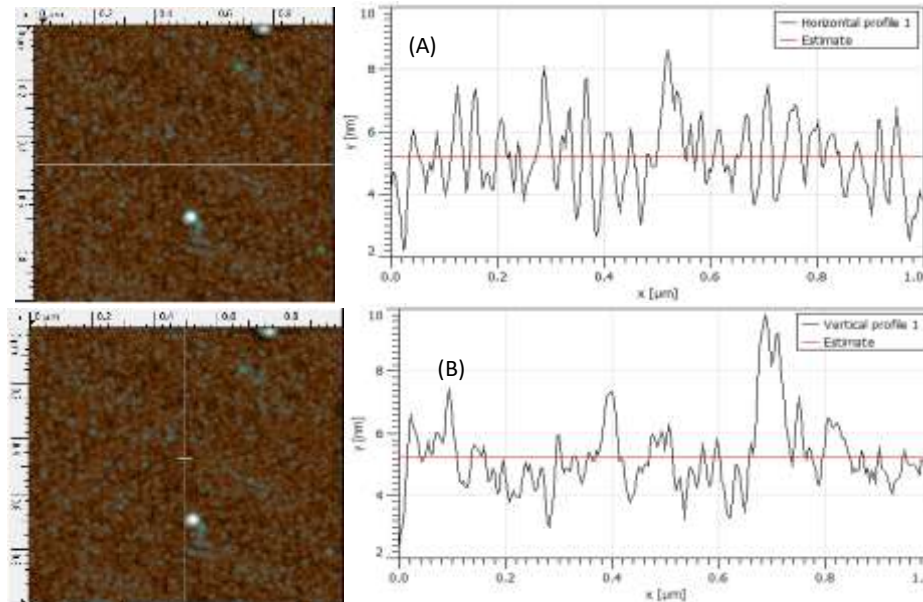


Figure 6 (A) horizontal profile and (B) vertical profile of the surface of the thin layer of the first sample.

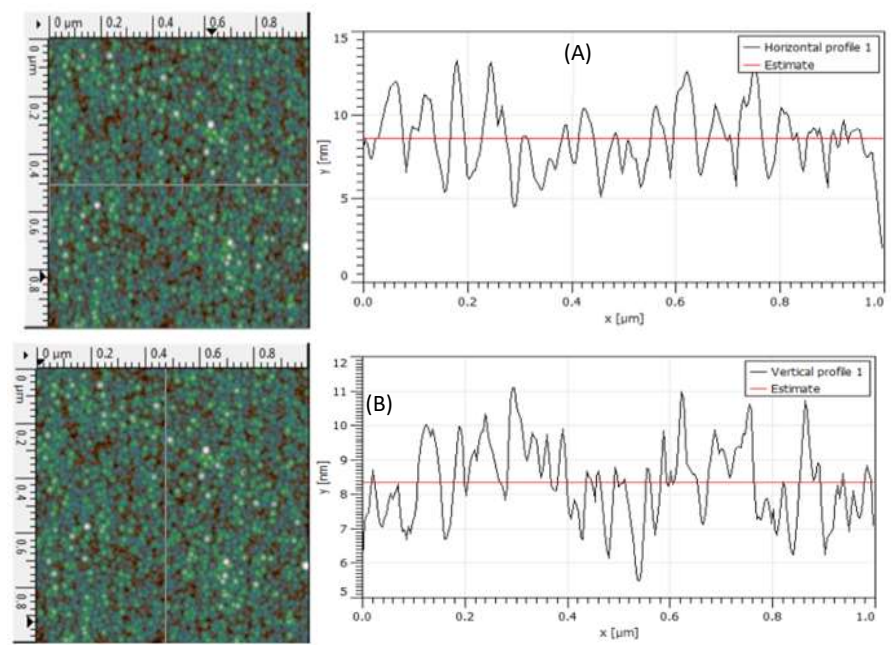
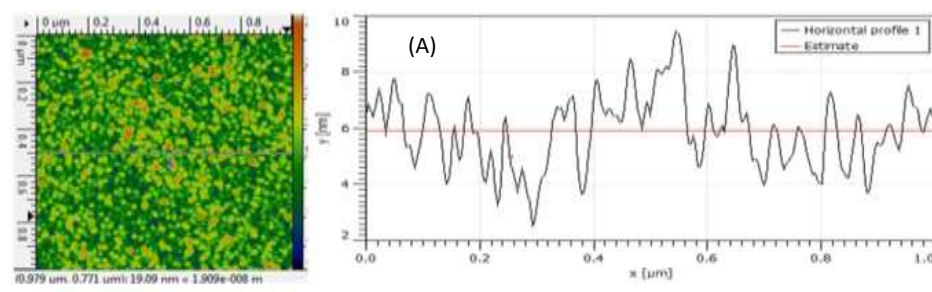


Figure 7 (A) horizontal profile and (B) vertical profile of the surface of the thin layer of the second sample.



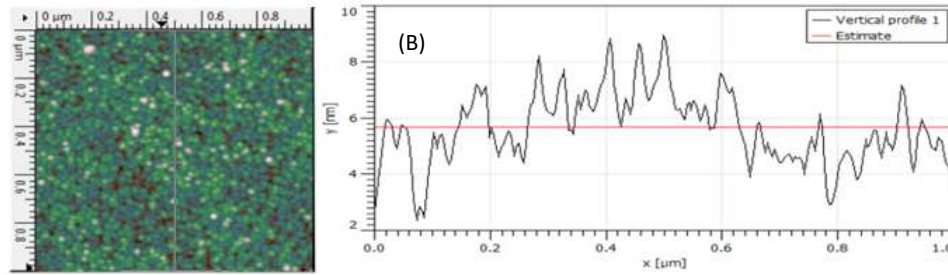


Figure 8 (A) is a horizontal profile, and (B) is a vertical profile of the surface of the thin layer of the third sample.

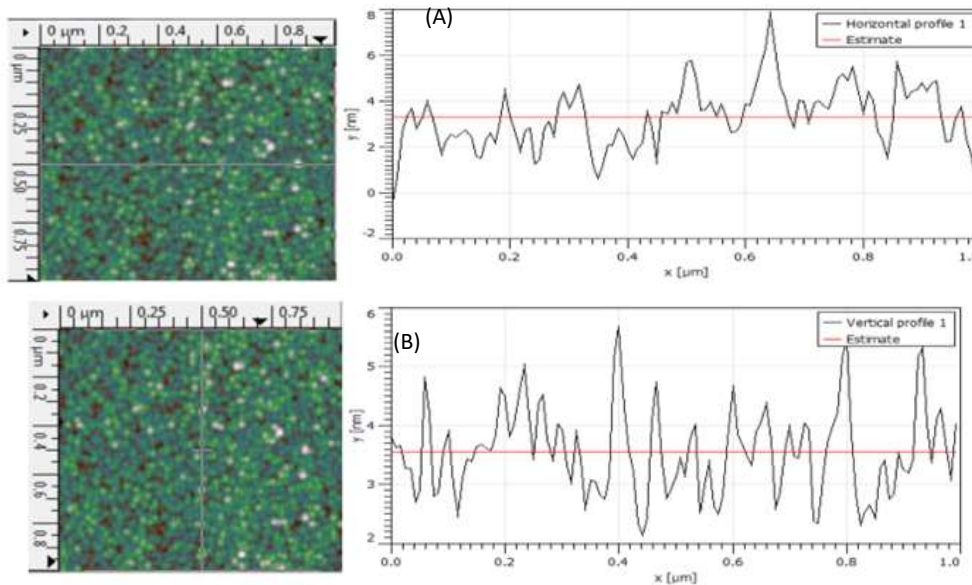


Figure 9 (A) is a horizontal profile, and (B) is a vertical profile of the surface of the thin layer of the fourth sample

5. Conclusion

The XRD outcome spectra show predominantly zinc and oxygen peaks, showing nature's Crystallinity, as shown in Figure 1. The ZnO nanostructures obtained are homogeneous and similar, which offer fine crystalline. All the samples have the highest peaks at an angle of approx 35°. These samples match well with standard card numbers 079-0207. The size of the crystals, depending on the dominant orientation, was calculated using Scherer's relation (Eq. 7). Figure 2 (A-D) shows the three-dimensional Atomic Force Microscope images of the surface of ZnO thin films annealed at 200°C, 300°C, 400°C, and 500°C. According to Figure 2, the size of the surface of all samples is 1μm×1μm, and the maximum height of the character is 60.5, 28.8, 29.0, and 32.5 nm, respectively. The roughness of the samples was analyzed using an Atomic Force Microscope and MATLAB software, and the results are listed in Table 3. Histograms of height distributions, which are approximately Gaussian distributions, along with their normal distributions, are plotted in Figure 3 A-D. In Figures 3 B and 3 C, a part of the distribution is placed to the left of the standard distribution curve, indicating negative skewness; that is, most sample materials are above the average level line. In Figure 3 D, a small part of the distribution is placed to the right of the standard distribution curve, which indicates positive skewness; that is, the majority of the sample materials are below the average level line, and in Figure 3 A, the sample distribution is almost consistent with the Gaussian (normal) distribution. , that is, the distribution of particles is practically uniform. It can be seen in Fig. 4 that the particle distribution on the sample surfaces during the coating process is almost constant, and about 80% of the data are located on the surface (mean line). Approximately 10% of the data are above the mean streak, and another 10% are below the mean line, resulting in surface roughness. The height-height correlation function graphs for the sample surfaces are shown in Figure 5. By fixing the charts and obtaining the intersection point between the smooth part of the curve and the inclined part of the graphs, the morphology of the surfaces is obtained according to equation (6). Ultimately, ZnO thin films were prepared on glass substrates using electron-beam physical vapor deposition at different deposition rates. X-ray diffraction analysis was performed to identify layer purity and determine grain size, and AFM analysis was used to describe the morphology of the thin films. Surface morphologies at different annealing temperatures were investigated, and the results indicate that temperature significantly affects surface morphology. Similar roughness values for all samples indicate that roughness formation dynamics may be similar. This deposition method allows access to thin films with desired thickness and roughness with sufficient accuracy.

Funding: This research received no external funding.

Conflicts of Interest: The authors declare no conflict of interest.

ORCID iD: 0009-0004-7073-231

Publisher's Note: All claims expressed in this article are solely those of the authors and do not necessarily represent those of their affiliated organizations, or those of the publisher, the editors and the reviewers.

References

- [1] Abegunde, O. O., Akinlabi, E. T., Oladijo, O. P., Akinlabi, S., & Ude, A. U. (2019). Overview of thin film deposition techniques. *AIMS Materials Science*, 6(2), 174-199. <https://doi.org/10.3390/ma6051584>
- [2] Aver'Yanova, I., Bogomolov, D., & Poroshin, V. (2017). ISO 25178 standard for three-dimensional parametric assessment of surface texture. *Russian Engineering Research*, 37(6). <https://doi.org/10.3103/S1068798X17060053>
- [3] Amakali, T., Daniel, L., Uahengo, V., Dzade, N. Y., & De Leeuw, N. H. (2020). Structural and optical properties of ZnO thin films prepared by molecular precursor and sol-gel methods. *Crystals*, 10(2), 132. <https://doi.org/10.3390/cryst10020132>
- [4] Bukhari, S. S., Vardaxoglou, J., & Whittow, W. (2019). A metasurfaces review: Definitions and applications. *Applied Sciences*, 9(13), 2727. <https://doi.org/10.3390/app9132727>
- [5] Butt, M. A. (2022). Thin-film coating methods: A successful marriage of high-quality and cost-effectiveness—A brief exploration. *Coatings*, 12(8), 1115. <https://doi.org/10.3390/coatings12081115>
- [6] Borysiewicz, M. A. (2019). ZnO as a functional material, a review. *Crystals*, 9(10), 505. <https://doi.org/10.3390/cryst9100505>
- [7] Benelmekki, M., & Erbe, A. (2019). Nanostructured thin films—background, preparation and relation to the technological revolution of the 21st century. In *Frontiers of Nanoscience* (Vol. 14, pp. 1-34). Elsevier. <https://doi.org/10.1016/B978-0-08-102572-7.00001-5>
- [8] Chen, X., Xie, Q., & Li, J. (2020). Significantly improved photoluminescence properties of ZnO thin films by lithium doping. *Ceramics International*, 46(2), 2309-2316. <https://doi.org/10.1016/j.ceramint.2019.09.220>
- [9] Guermat, N., Daranfed, W., Bouchama, I., & Bouarissa, N. (2021). Investigation of structural, morphological, optical and electrical properties of Co/Ni co-doped ZnO thin films. *Journal of Molecular Structure*, 1225, 129134. <https://doi.org/10.1016/j.molstruc.2020.129134>
- [10] Ghule, K., Ghule, A. V., Chen, B. J., & Ling, Y. C. (2006). Preparation and characterization of ZnO nanoparticles coated paper and its antibacterial activity study. *Green Chemistry*, 8(12), 1034-1041.
- [11] Hobson, R. D. (2019). Surface roughness in topography: quantitative approach. In *Spatial analysis in geomorphology* (pp. 221-246). Routledge.
- [12] Henniges, U., Hasani, M., Potthast, A., Westman, G., & Rosenau, T. (2013). Electron beam irradiation of cellulosic materials—opportunities and limitations. *Materials*, 6(5), 1584-1598. <https://doi.org/10.3390/ma6051584>
- [13] Kayani, Z. N., Sahar, M., Riaz, S., Naseem, S., & Saddiqe, Z. (2020). Enhanced magnetic, antibacterial and optical properties of Sm doped ZnO thin films: role of Sm doping. *Optical Materials*, 108, 110457. <https://doi.org/10.1016/j.optmat.2020.110457>
- [14] Lee, J. H., Ko, K. H., & Park, B. O. (2003). Electrical and optical properties of ZnO transparent conducting films by the sol-gel method. *Journal of crystal growth*, 247(1-2), 119-125. [https://doi.org/10.1016/S0022-0248\(02\)01907-3](https://doi.org/10.1016/S0022-0248(02)01907-3)
- [15] Manesh, K. K., Ramamoorthy, B., & Singaperumal, M. (2010). Numerical generation of anisotropic 3D non-Gaussian engineering surfaces with specified 3D surface roughness parameters. *Wear*, 268(11-12), 1371-1379. <https://doi.org/10.1016/j.wear.2010.02.005>
- [16] Mehmood, B., Khan, M. I., Iqbal, M., Mahmood, A., & Al-Masry, W. (2021). Structural and optical properties of Ti and Cu co-doped ZnO thin films for photovoltaic applications of dye sensitized solar cells. *International Journal of Energy Research*, 45(2), 2445-2459. <https://doi.org/10.1002/er.5939>
- [17] Salditt, T., Metzger, T. H., Peisl, J., Reinker, B., Moske, M., & Samwer, K. (1995). Determination of the height-height correlation function of rough surfaces from diffuse X-ray scattering. *Europhysics Letters*, 32(4), 331. DOI: 10.1209/0295-5075/32/4/008
- [18] Viswanathan, K., Shyju, T. S., Ramachandran, D., & Pradhaban, G. (2016). Electric properties of ZnO thin films by RF Magnetron sputtering technique. *Materials Today: Proceedings*, 3(6), 1548-1552. <https://doi.org/10.1016/j.matpr.2016.04.041>
- [19] Xu, C., Anusuyadevi, P. R., Aymonier, C., Luque, R., & Marre, S. (2019). Nanostructured materials for photocatalysis. *Chemical Society Reviews*, 48(14), 3868-3902. <https://doi.org/10.1039/C9CS00102F>
- [20] Xia, C., Pan, Z., Polden, J., Li, H., Xu, Y., & Chen, S. (2022). Modelling and prediction of surface roughness in wire arc additive manufacturing using machine learning. *Journal of Intelligent Manufacturing*, 1-16.